Available online at www.sciencedirect.com
SCIENCE DIRECT®
International Journal of Heat and Mass Transfer 47 (2004) 4301–4314
International Journal of HEAT and MASS TRANSFER
www.elsevier.com/locate/ijhmt

Enhancement of convective heat transfer in the developing region of circular tubes using corona wind

Majid Molki *, Kanthi Latha Bhamidipati [1]

Department of Mechanical and Industrial Engineering, Southern Illinois University-Edwardsville, Edwardsville, IL 62026-1805, USA

Received 31 December 2003; received in revised form 23 April 2004
Available online 26 June 2004

Abstract

An experimental research was conducted to investigate the level of heat transfer enhancement that can be achieved by corona wind in the developing region of circular tubes. The study was focused on transitional and lower range of turbulent flows with Reynolds number and voltage ranging from 2500 to 13 000 and 0 to 10.5 kV, respectively. The maximum enhancements of the local and average heat transfer coefficients were 14–23% and 6–8%, respectively. These values indicate the level of enhancement beyond the conventional values in the developing region of the circular tubes.

Keywords: Corona wind; Air; Heat transfer; Enhancement; Tube

1. Introduction

Under an intense electric field, air partially breaks down and becomes a conductor. Under these conditions, air is ionized and results in corona discharge. Corona is a visible luminous emission caused by creation of photons. This occurs in the vicinity of sharp edges where the intensity of electric field is high. The electric current associated with the corona discharge is small in heat transfer enhancement applications and is normally of the order of milliamps.

An important aspect of corona discharge is the generation of corona wind. This phenomenon is caused by the ionization of air molecules and formation of electrons that accelerate in strong electric fields and collide with neutral molecules, resulting in more ionization. The ions are heavier than electrons; they accelerate and drag the neighboring air molecules. This results in formation of a secondary flow, known as corona wind. In this research, we used corona wind to enhance heat transfer in the developing region of a tube.

There are two main groups of research in corona. The first group is focused on the characteristics of corona discharge. The second is concerned with its application in heat transfer enhancement. These studies are summarized in Tables 1 and 2.

Review of the literature reveals special features of corona discharge. The corona current and ion mobility both decrease with relative humidity [1–3]. In a barbed plate-to-plane arrangement, the maximum current density (A/m^2) depends on tip-to-plate spacing and the applied voltage [4]. In co-axial electrode arrangement in pipes, on the other hand, high flow rates cool the electrode surface, stabilize the discharge, and increase the current [5,6]. It has been shown that humidity affects the corona onset voltage [7]. The onset voltage increases with humidity up to a certain point, after which it begins to decrease. In multi-point electrode systems, air velocity has an increasing effect on corona onset voltage [8]. When electrodes are placed parallel or perpendicular to air flow, corona onset voltage is independent of

* Corresponding author. Tel.: +1-618-650-2372; fax: +1-618-650-2555.
E-mail addresses: mmolki@siue.edu (M. Molki), kanthilatha.bhamidipati@ge.com (K.L. Bhamidipati).
[1] Present address: GE India Technology Centre Pvt. Ltd., 122 EPIP Phase 2, Hoodi Village, Whitefield Road, Bangalore 560 066, India.

0017-9310/$ - see front matter
doi:10.1016/j.ijheatmasstransfer.2004.04.014

Nomenclature

A	tube cross-sectional area, $\pi D^2/4$
D	tube inside diameter
f	friction factor
h	convective heat transfer coefficient
I	electric current
k	thermal conductivity
K_p	pressure coefficient, Eq. (6)
Ne	electric number, Eq. (9)
Nu	Nusselt number, hD/k
P	air pressure
Pr	Prandtl number
q''	heat flux
Q	rate of heat transfer
Re	Reynolds number, $\rho VD/\mu$
T	temperature
V	mean velocity, voltage
x	axial coordinate, $x = 0$ indicates the tube inlet

Greek symbols

β	ion mobility for positive ions, 1.4×10^{-4} m^2/(V s)
μ	air viscosity
ρ	air density

Subscripts

ave	average value
bulk	bulk value
c	corona
fd	fully developed value
L	loss
0	at the first pressure tap, zero voltage
r	local value at radial location r
wall	wall value
x	local value at axial location x

magnitude and direction of flow for all polarities [9]. For a given voltage, however, corona current increases with velocity up to an extent, and then it decreases.

Corona wind has been used effectively in a number of studies to enhance heat transfer. In pipes with a co-axial electrode, the maximum enhancement at $Re = 2000$ is 215% [10]. This high enhancement is obtained when the electrode power is included in the total heat transfer from the tube surface. In more complex geometries, such as a heat exchanger, the enhancement is less. In co-axial shell-and-tube heat exchangers, for example, the maximum enhancement of 35% at $Re = 4000$ on the shell side showed only 22% increase on the tube side at the same Reynolds number [11]. When electrodes are placed parallel or perpendicular to air flow in a channel, the Nusselt number increases with the applied voltage at lower Reynolds numbers [12]. In general, the corona wind effect on heat transfer diminishes as flow Reynolds number increases. In corona wind cooling of cylinders, multi-point electrodes result in higher enhancement than single-point electrodes [13]. This technique can also be used to enhance heat transfer in laminar mixed convection flows where buoyancy force is present. In this connection, when a positively charged electrode is placed at the center of a horizontal channel, temperature and flow fields are stable at low voltages; but the fields become oscillatory at higher voltages [14]. In wire-plate geometry, negative polarity gives higher current and lower corona wind [15], and the maximum heat transfer enhancement occurs right below the electrode. In cross-flow air heat exchangers, enhancement is higher in the laminar regions [16].

The present research is on enhancement of heat transfer in the developing region of tubes using corona wind. The local information for this region of circular tubes is seemingly non-existent in the published literature. In the experiments, a wire electrode was placed at the center of a grounded aluminum tube, and it was charged with 0–10.5 kV high voltage. The Reynolds number for air flow inside the tube ranged from 2500 to 13 000, which corresponded to transitional and lower range of turbulent flows. The corona wind generated by the charged electrode created a secondary flow that enhanced the heat transfer. The enhancement was more prominent in flows with lower Reynolds numbers. The local heat transfer enhancement, relative to the local values, varied from 23% at $Re = 2500$ to 14% at $Re = 13\,000$. These maximum enhancements occurred at the downstream end of the tube and corresponded to the applied voltage of 10.5 kV. The enhancement was found to decrease with increasing Reynolds number.

2. Experimental setup and procedure

The experimental setup used in this investigation is shown in Fig. 1. The main components of the setup are: test section, exhaust tube, charged electrode, rotameter, and blower. A high-voltage DC power supply was used to charge the electrode. An AC power supply was used to run the variable-speed blower and another power supply provided electrical power to the heating wire of the test section. Data Acquisition System recorded the thermocouple and pressure transducer readings.

Table 1
Review of the literature on corona discharge

Author	Application	Type of analysis	Geometry	Range of parameters	Remarks
Robledo-Martinez [1]	Corona discharge dependency on humidity	Experimental	Point-plane arrangement	$43\% \leqslant RH \leqslant 68\%$	Current ↓ when RH ↑, ion mobility ↓ when RH ↑, More rigorous streamers in dry air compared to dry air
McKinney et al. [4]	Corona current density distributions	Experimental and numerical	Barbed plate-to-plane arrangement	$1 \leqslant$ barbs $\leqslant 9$ $5.5 \leqslant$ length $\leqslant 25.5$ mm $7.6 \leqslant$ space $\leqslant 12.8$ mm	Max current density depends on tip-to-plate spacing and applied voltage. Current density uniformity depends on barb length and barb spacing
Adamiak et al. [24]	Effect of shaped electrodes on corona current distribution	Experimental and numerical	Shaped electrodes-cylinder geometry	Wire dia = 0.1 mm Wire length = 20 mm	Current ↓ when termination diameter ↑ Current ↑ when Voltage ↑
Chang et al. [5]	Effects of gas inlet temperature and flow rate on corona discharge	Experimental	Co-axial electrode in pipe	$10 \leqslant$ inlet $T \leqslant 60$ °C $-10 \leqslant V_0 \leqslant 10$ kV	If T ↑, then discharge instability ↑ and current ↓. High flow rate cools electrode surface, stabilize the discharge, and increases current due to the discharge uniformity
Fouad and Elhazek [7]	Effect of humidity on corona discharge	Experimental	Three-electrode arrangement	Not reported	Corona onset voltage ↑, with humidity ↑ to an extent and then ↓
Jaworek and Krupa [8]	Effects of flowing air on corona discharge	Experimental	Multi-point electrode system	$0 \leqslant$ air velocity $\leqslant 4$	Corona onset ↑, as velocity ↑ Breakdown streamer voltage ↑, as velocity ↑
Calva and Espino [2]	Effect of relative air density and humidity on corona discharge	Experimental	Rod-plane arrangement	$10 \leqslant$ gap $\leqslant 100$	Ionic mobility ↓, as relative density ↑ Current ↓, as humidity ↑ Current ↓, as gap ↑
Jeong and Kim [25]	Electrohydrodynamic flow in a rectangular impactor using corona discharge	Experimental and numerical	Rectangular impactor	$500 \leqslant Re \leqslant 2500$	Current density is found to be higher right below the discharge electrode and decreased towards the end of the plate. Velocity of the discharge wind is maximum at the axis and decreased towards the throat wall
Kondratov et al. [26]	Impulse corona discharge current characteristics	Experimental	Co-axial wire-cylinder geometry	$15 \leqslant$ Voltage $\leqslant 35$	Current stabilizes much faster in low voltage and low current cases
Asono et al. [27]	Characteristics of DC corona discharge	Experimental	Parallel-plate electrode arrangement	Not reported	Corona onset voltage ↑ when filament particle ↓, corona onset voltage ↓in negative discharge
Abdel-Salam et al. [28]	Influence of geometry on corona discharge characteristics	Experimental	Co-axial wire-cylinder and co-axial wire-duct reactors	0.025 mm $\leqslant$ wire radius $\leqslant$ 0.2 mm	Onset voltage is found to be same for AC corona and silent discharges. Onset voltage ↑ in co-axial wire-duct reactors. Current higher in wire-cylinder arrangement
Yehia et al. [9]	Effect of magnitude and direction of airflow on corona discharge	Experimental	Electrodes placed parallel and perpendicular to airflow between stainless steel plates	294 K $\leqslant$ atmospheric temperature $\leqslant$ 296 K	Corona onset voltage is independent of magnitude and direction of flow for all polarities. For a given voltage, corona current ↑ up to an extent with velocity and then ↓
Zebboudj and Ikene [29]	Effect of air density and humidity conditions on positive corona inception	Experimental	Wire-cylinder and wire-plane geometries	Not reported	Corona inception voltage ↑ as humidity ↑ corona range ↓ as humidity ↓
Leger et al. [3]	Effect of corona discharge on a flat plate	Experimental	Three different cathode, anode arrangements separated by 4-cm gap	$41\% \leqslant RH \leqslant 49\%$	Corona current ↑ as humidity ↓

Table 1 (*continued*)

Author	Application	Type of analysis	Geometry	Range of parameters	Remarks
Toyota et al. [30]	Electrical discharge characteristics in air and nitrogen at cryogenic temperature	Experimental	Sphere-to-sphere and rod-to-plane arrangement	20 mm $\leqslant$ sphere–sphere gap $\leqslant$ 150 mm 20 mm $\leqslant$ sphere–sphere gap $\leqslant$ 330 mm	Breakdown voltages depend on the product of gap length and gas density and found to be independent of temperature
Hoshino et al. [6]	Effect of airflow and air-isopar mixture on corona discharge	Experimental	Co-axial wire-cylinder geometry	Not reported	Corona current ↑ as air velocity ↑

Details of the test section are shown in the lower diagram of Fig. 1. The test section was an extruded 6061-T6 aluminum alloy tube ($\rho = 2712$ kg/m^3, $k = 167$ W/mK). The inner diameter, wall thickness, and length of the tube were, respectively, 25.4, 6.35, and 304.8 mm. A stainless steel electrode wire having a diameter of 0.254 mm was placed at the center of the test section tube and was charged with positive high voltage. The aluminum tube was grounded. The choice of the inner diameter of the test section tube was based on the electric field intensity between the tube and electrode. A large-diameter tube would reduce the electric field intensity and weaken the corona wind. On the other hand, if the tube diameter were too small, spark would occur earlier at lower voltages.

In order to minimize the heat conduction losses from the upstream and downstream ends of the test section, Teflon disks ($\rho = 2150$ kg/m^3, $k = 0.35$ W/mK) were mounted on either end of the test section tube. The disks had the same inner diameter as the inner diameter of the tube, but their outer diameter was 50.8 mm. The disks were allowed to slide over the test section with no gap in between. The thicknesses of the Teflon disks located on the upstream and downstream ends of the test section were, respectively, 12.7 and 50.8 mm. The thickness difference of disks was necessary, as there was higher heat loss from the much hotter downstream end of the test section. With this arrangement, the effective length of the test section, i.e. the total tube length minus the length covered by the Teflon disks, was 288.29 mm. In order to prevent the downstream hydrodynamic effects, the test section was extended by a piece of adiabatic exhaust tube. This tube was also made of aluminum and had the same inner and outer diameters. The length of the exhaust tube was 355.6 mm.

A nichrome heating wire was wrapped around the test section with a pitch distance of 5 mm. This pitch was good enough to provide a nearly uniform heating on the outer surface of the test section tube. The heating wire was powered by a variable AC power supply that could provide 0–132 V. The maximum current was 3 A. Voltage across the test section heater was measured by a Fluke multimeter connected in parallel. The currents were measured by a similar multimeter connected in series.

Holes were drilled into the tube wall to a depth of 5.55 mm to position the thermocouple junctions to within 0.8 mm from the inner surface of the tube (Fig. 1). On the opposite side of the thermocouples, the pressure taps were drilled into the tube wall for pressure measurement. A 0–103.4 kPa differential pressure transducer was used to measure the pressure drop along the tube.

To control the convection losses from the test section and other components, foam insulation and fiberglass insulation were used. Two layers of foam insulation

Table 2
Review of the literature on enhancement of heat transfer by corona wind

Author	Application	Type of analysis	Geometry	Range of parameters	Remarks
Ohadi et al. [10]	EHD enhancement of heat transfer in circular pipes	Experimental	Co-axial electrode in pipe, and two electrodes in pipe	$1000 \leqslant Re \leqslant 20000$ $6 \leqslant$ Voltage $\leqslant 7.75$	Max enhancement of 215% occurs in transitional flow, $Re = 2000$. For $Re = 1000$, enhancement drops at high voltage
Ohadi et al. [11]	EHD enhancement of heat transfer in a shell and tube heat exchanger	Experimental	Co-axial shell and tube exchanger with concentric electrode in the tube and four electrodes on shell side	$0 \leqslant \text{Voltage}_{\text{tube}} \leqslant 7.75$ $0 \leqslant \text{Voltage}_{\text{shell}} \leqslant 17.75$	Maximum enhancement of 35% on shell side at a Reynolds number of 4000 showed an increase of 22% on tube side
Takimoto et al. [31]	Heat transfer enhancement in channel flow	Experimental	Single-wire electrodes and two-wire electrodes placed perpendicular to flow in a channel	$0 \leqslant Re \leqslant 1170$	Current density is higher right below the wires, and that the current density is lowered in the case of two-wire electrode system Primary velocity ↑ secondary flow ↓
Tada et al. [12]	Heat transfer enhancement	Experimental	Electrodes placed parallel or perpendicular to air flow in a channel	$900 \leqslant Re \leqslant 2000$ $0 \leqslant$ Voltage $\leqslant 12$	Nusselt number ↑ as voltage ↑ Nusselt number ↑ as Reynolds number ↓
Blanford et al. [32]	Effect of enhancement of airside heat transfer in cross-flow refrigerant-to-air heat exchanger	Experimental	Cross-flow refrigerant-to-air heat exchanger	$1000 \leqslant Re \leqslant 3000$	Temperature difference between heat exchanger surface ↓ heat transfer enhancement ↑
Franke and Hodge [13]	Corona wind cooling of cylinders	Experimental	Three different cylinders with three different EHD enhancement arrangements	$0 \leqslant$ Voltage $\leqslant 14$	Multi-point electrode results in higher enhancement than single point electrode. Corona wind heat transfer enhancement is less than heat transfer enhancement using air jets
Yang et al. [33]	Effect of Joule heating on EHD-enhanced natural convection	Experimental	Rectangular channel with walls maintained at different temperatures	$0 \leqslant$ Voltage $\leqslant 17.75$	Joule heating increases heat transfer, but heat rejection to the wall is a disadvantage
Lai [14]	Buoyancy effect on EHD-enhanced convection in a horizontal channel	Numerical	Positively charged electrode placed at the center of horizontal channel	$600 \leqslant Re \leqslant 1800$ $10 \leqslant$ Voltage $\leqslant 17.5$	At low voltages, temperature and flow fields are stable, but as voltage increases, fields become oscillatory
Nelson et al. [22]	Effect of corona discharge on heat transfer enhancement and pressure drop in pipes	Experimental	Co-axial wire-cylinder geometry	$1000 \leqslant Re \leqslant 20000$ $6 \leqslant$ Voltage $\leqslant 7.75$	Positive discharge and double-electrode arrangement are more effective in heat transfer enhancement than negative discharge and single-electrode arrangement
Kalman and Sher [15]	Effect of applying corona wind on enhancement of heat transfer using corona wings assembly	Experimental	Wire-plane geometry	Not reported	Negative polarity gives higher current and low corona wind velocity. Heat transfer enhancement is maximum right below the electrode As Reynolds number ↑ enhancement↑
Molki et al. [34]	Airside heat transfer enhancement using EHD technique in duct flows	Experimental and numerical	Co-axial wire-duct geometry	$500 \leqslant Re \leqslant 2000$ $-5.655 \leqslant V_0 \leqslant -6.9$ kV	Fully developed flow has max. enhancement of 3.4. Developing flow has heat transfer enhancement from 1.56 to 2.01

Table 2 (*continued*)

Author	Application	Type of analysis	Geometry	Range of parameters	Remarks
Ngo and Lai [35]	Natural convection	Numerical	An electrode at the center of a high aspect ratio enclosure	$10^3 \leqslant Ra \leqslant 10^6$ $12 \leqslant V_0 \leqslant 18$ kV	Flow becomes steady, periodic steady, or non-periodic. Steadiness of the flow increases with voltage and Ra. Max. enhancement is 13 times
Tan and Lai [36]	Natural convection	Numerical	An electrode placed in various locations inside an enclosure	$10^3 \leqslant Ra \leqslant 10^6$ $12 \leqslant V_0 \leqslant 18$ kV	When uniformity of electric field ↑, heat transfer enhancement ↑ Max. enhancement is 21 times
Kasayapanand et al. [37]	Effect of Corona discharge on heat transfer enhancement in a tube bank cross-flow heat exchanger	Numerical	Tube bank with six different electrode arrangements	$100 \leqslant Re \leqslant 1500$ $7.5 \leqslant V_0 \leqslant 17.5$ kV	Nusselt number increases gradually as fluid moves from upstream end to downstream end Enhancement is higher in laminar regions as compared to turbulent regions
Wangnipparnto et al. [16]	EHD enhancement on airside in a thermosyphon heat exchanger	Experimental	Cross-flow refrigerant-to-air heat exchanger	$58 \leqslant Re \leqslant 230$ $15.5 \leqslant V_0 \leqslant 17.5$ kV	Enhancement is higher in laminar regions as compared to turbulent regions Enhancement is 15% at Reynolds number of 58

(12.7 mm thick, $k = 0.036$ W/mK) and two layers of fiberglass insulation (50.8 mm thick, $k = 0.046$ W/mK) were wrapped around the test section and exhaust tubes. The exhaust tube was connected to the rotameter by PVC fittings. A suction blower was mounted at the downstream end of the rotameter using a connection hose. This arrangement allowed the blower to operate in suction mode, to draw the laboratory air into the test section, and to prevent unwanted heating of the incoming air by the heat of blower. The blower speed was controlled by a 0–140 V, variable AC power supply. The power supply could provide a maximum current of 10 A.

The electrode was an 889-mm-long stainless steel wire. The electrode ran concentrically through the test section, exhaust tube, and the PVC fittings. The electrode was tightly held in tension using a support fixture. The electrode wire was bare inside the test section, and it was electrically insulated elsewhere. The diameter of the electrode was deliberately maintained very small (0.254 mm) to generate corona discharge. The voltage applied to the electrode was a positive DC voltage. The ranges of voltage and current of the high-voltage power supply were 0–30 kV and 0–20 mA, respectively. The voltage and current were measured by Fluke multimeters.

Temperatures were measured by T-type thermocouples, calibrated prior to the experiments. The calibrations estimated the fixed and bias errors of each thermocouple. The calibration was performed in a constant-temperature water bath (Hart Scientific, Model 7012) for 20–50 °C. During the calibration, the constant temperature bath was maintained at the calibration temperature to within ±0.001 °C. The bath temperature was measured by a thermistor diode. The thermocouples to be calibrated were immersed simultaneously in the water bath and were kept close to the probe and the temperature measured by each thermocouple was recorded by a Data Acquisition System for 30 min maintaining a span of 10 s between two successive readings. The entire process was repeated one more time, and the average of the two readings was taken. The difference between the actual water bath temperature and the average of the measured temperatures gave the bias error. Precision error was estimated as twice the standard deviation of the thermocouple readings. The average values of precision and bias errors for all thermocouples used in the experiments were $2\sigma = 0.06$ and 0.45 °C, respectively, where σ is the standard deviation.

In the heat transfer experiments, the air flow rate was set and the test section tube was heated. The first experiment was performed with no voltage applied to the electrode. It took approximately 90 min for the experiment to reach steady state. To ensure this, the experiment was continued by another hour until the thermocouple readings almost remained the same. At this time, the temperatures and the flow rate were re-

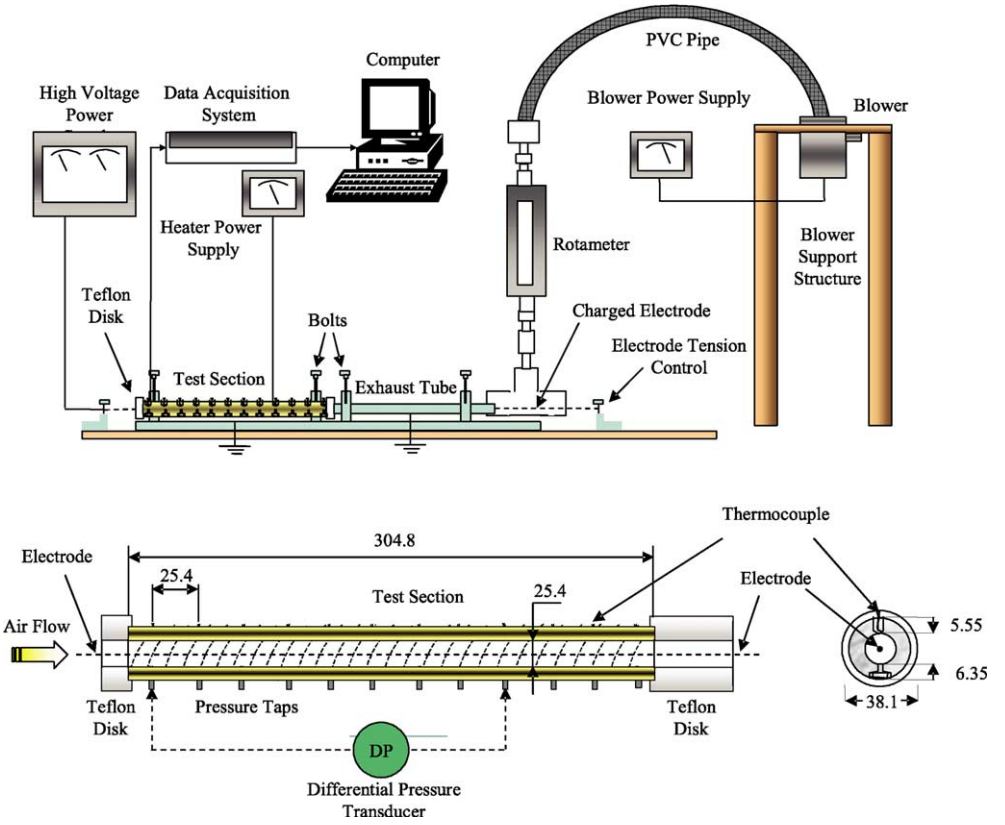

Fig. 1. The experimental setup; dimensions are in mm.

corded. This procedure was repeated for the case of charged electrode. In this case, the experimental run started by applying a high voltage that was below, but very close to, the threshold (corona onset) voltage. Voltage was gradually increased to a value close to the spark limit. The temperatures were scanned using a Data Acquisition System and were recorded on a computer. This procedure was repeated for different flow rates corresponding to Reynolds numbers ranging from 2500 to 13 000. Pressure drop along the tube was also measured. A 2-mmHg pressure transducer was used for tests at low Reynolds numbers, while a 10-mmHg transducer was used for other tests. Pressures were recorded by the Data Acquisition System.

3. Data reduction

The local heat transfer coefficient, h_x, is equal to

$$h_x = \frac{q''_x}{T_{\text{wall},x} - T_{\text{bulk},x}} \tag{1}$$

where q''_x is the heat flux transferred to air, and $T_{\text{wall},x}$ and $T_{\text{bulk},x}$ are the local wall and bulk temperatures.

Despite the nearly uniform heat flux provided by the wraps of heating wire to the outer surface of the test section tube, the heat flux at the inner surface of the tube was not uniform due to axial heat conduction along the tube wall. Thin boundary layer of air near the tube inlet demanded more heat and encouraged the axial wall conduction to provide this heat. To account for wall conduction and non-uniformity of heat flux at the inner surface of the tube, local heat flux, q''_x, was determined from a computational model using FLUENT software. The computational domain included the test section, the exhaust tube, and the air. The upstream boundary was far away from the tube inlet, while the downstream boundary was placed at the end of the exhaust tube. In the radial direction, the boundary was positioned at the outer surface of the tube where heating wire was located; the inner boundary was at the tube centerline. With this arrangement, the computations were performed as a conjugate problem that took into account the conduction through the tube walls as well as convection in air. The experimental data were given as input to the software, and the heat flux distribution for the inner surface was determined.

The local wall temperature, $T_{\text{wall},x}$, was already available for the points where surface temperature had been measured. However, the values of this temperature at other axial locations as needed for computation of the

local heat transfer coefficient was determined from the least-squares curve fitting of the measured wall temperatures.

The local air bulk temperature, $T_{\text{bulk},x}$ was determined from energy balance at the tube cross-section located a distance x from the inlet.

$$T_{\text{bulk},x} = \frac{1}{AV}\int V_r T_r \, \mathrm{d}A \tag{2}$$

In this equation, V and V_r are the mean and local velocities, T_r is air temperature at radial position r, and $A = \pi D^2/4$ is the cross-sectional area of the tube.

In addition to local heat transfer coefficient, h_x, average heat transfer coefficients for the length of tube from $x = 0$ (inlet) to x was calculated from energy balance according to

$$h_{\text{ave}} = \frac{(1/x)\int_0^x q''_x \, \mathrm{d}x}{T_{\text{wall,ave}} - \frac{T_{\text{bulk,in}} + T_{\text{bulk,out}}}{2}} \tag{3}$$

Once the heat transfer coefficients were determined, the local and average Nusselt numbers were obtained from the conventional definitions

$$Nu_x = \frac{h_x D}{k} \tag{4}$$

and

$$Nu_{\text{ave}} = \frac{h_{\text{ave}} D}{k} \tag{5}$$

where D and k are the tube inside diameter and air thermal conductivity. The experimental data will be presented in terms of Reynolds number defined as $Re = \rho V D/\mu$.

The pressure drops were also measured and were used to determine pressure coefficients as

$$K_{\text{p}} = \frac{P_0 - P_x}{0.5\rho V^2} \tag{6}$$

In this equation, P_0, P_x, ρ, and V are, respectively, pressure at the first tap, pressure at a distance x from the first tap, air density, and air mean velocity.

4. Experimental uncertainty

The experimental uncertainty of the present work was determined from the ASME guidelines on reporting uncertainties in experimental measurements [17,18]. The precision error, P_h, for each measured parameter, based on 95% confidence interval, was estimated as: Corona voltage, V_{corona} (±1% of the reading), Corona current, I_{corona} (±1% of the reading), Test section voltage, V_{test} (±1% of the reading), Test section current, I_{test} (±1% of the reading), Wall temperature, T_{wall} (±0.1 °C), and Air inlet temperature, T_{in} (±0.1 °C). Calibration of thermocouples indicated $2\sigma = 0.06$ °C, implying that the precision error of temperature measurement was ±0.06 °C. However, in the uncertainty analysis we used a more conservative value of ±0.1 °C as the precision error of thermocouples.

The bias error, B_h, for thermocouples was zero, because they had been calibrated. The bias error of other parameters was considered negligible. The theory of propagation of uncertainty was applied to evaluate the errors in the final results as $\Delta_h = \sqrt{P_h^2 + B_h^2}$ with $B_h = 0$ as explained earlier. The uncertainty bars are affixed to the data in some of the graphs to be discussed later in this paper.

5. Results and discussion

In order to test the data reduction procedure, the computational method was applied to a single tube without corona wind to reproduce the results reported by Sparrow and Molki [19]. We assumed an isothermal tube to simulate their mass transfer experiments. The Sherwood number data of [19] were converted to Nusselt number via $Nu = (Pr/Sc)^{0.37} Sh$ with $Pr = 0.71$ and $Sc = 2.5$. Two values of Reynolds number were considered, namely, $Re = 5000$ and 9000, which were close to the range of Reynolds numbers used in the present experiments (Fig. 2).

The results were also compared with those of Kays and Crawford [20]. The plot in [20] is given as Nu_x/Nu_{fd} for $Re \approx 50\,000$ for sharp-edge inlets similar to the inlet geometry of the present work. However, since Nu_x/Nu_{fd} is less dependent on Re than Nu_x, the values of Nu_x at $Re = 5000$ and 9000 were extracted by multiplying Nu_x/Nu_{fd} of [20] by the corresponding fully-developed values, Nu_{fd}, obtained from Gnielinski's correlation [21].

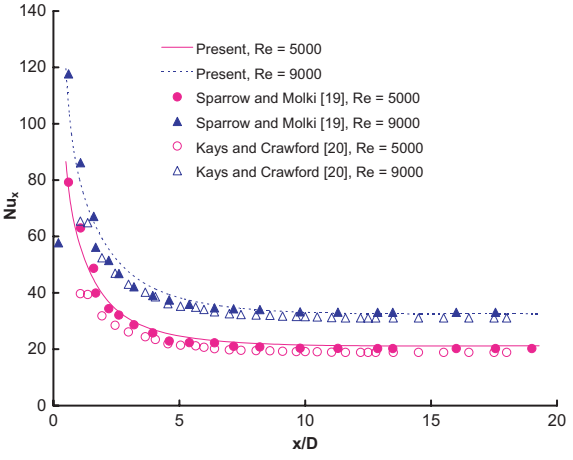

Fig. 2. Comparison of single tube results with the literature.

$$Nu_{fd} = \frac{(f/8)(Re - 1000)Pr}{1 + 12.7(f/8)^{1/2}(Pr^{2/3} - 1)} \quad (7)$$

In this equation, the friction factor is given by $f = (0.790 \ln Re - 1.64)^{-2}$. Eq. (7) is valid for $0.5 < Pr < 2000$ and $3000 < Re < 5 \times 10^6$, and it is applicable to air for this comparison. The good agreement seen in Fig. 2 validates the present data reduction procedure.

The effect of corona wind on heat transfer coefficient is shown in Fig. 3. In these figures, the ordinate is local Nusselt number divided by the fully developed Nusselt number obtained from Eq. (7) at the same Reynolds number. The abscissa is the distance from the tube inlet divided by tube inside diameter. Each plot corresponds to a fixed Reynolds number, with the applied voltage appearing as a parameter. In addition to $Re = 2500$ and 13 000, the experiments were also performed for $Re = 4000$, 7000, and 10 000. Here, we only present the results for the first two Reynolds numbers as they are the limiting cases.

The large values of heat transfer coefficient near the inlet and rapid decrease of the values along the flow is the well-known characteristics of the developing region. However, the question here is whether the corona wind is able to enhance this coefficient beyond the conventional value. As seen in Fig. 3, the enhancement begins farther away from the inlet after the coefficients have somewhat decreased. For all the Reynolds numbers, the level of enhancement increases with the applied voltage. As the voltage is increased, the ions move faster due to the higher intensity of the electric field, resulting in more collision and ionization. Moreover, faster ions carry larger momentum, drag the fluid particles, and result in higher heat transfer enhancement.

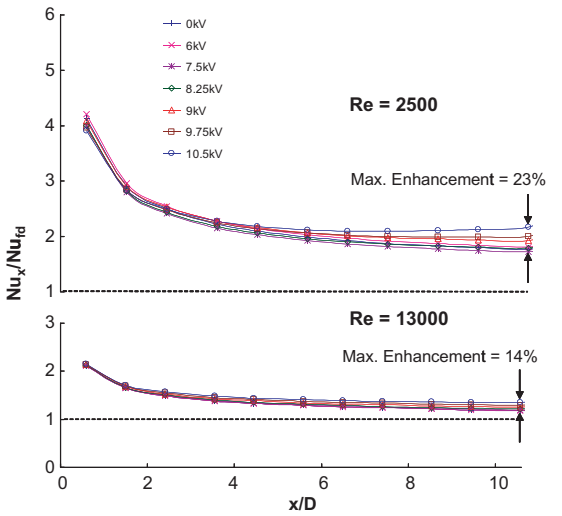

Fig. 3. Variation of the local Nusselt number in the developing region of the circular tube.

Reynolds number was found to have an inverse relationship to heat transfer enhancement. The ions are more effective in imparting momentum to slow-moving particles, as in low-Reynolds number cases. But as the fluid momentum increases with Reynolds number, the ions cannot be as effective in generating extra momentum and secondary motion. Thus the level of enhancement is reduced. Another explanation is that, the heat transfer coefficients in the turbulent flow are already high, and the corona wind cannot enhance the heat transfer beyond this high value.

In this research, the maximum enhancement was obtained at the end of the tube where the heat transfer coefficient for 0 kV (base case) was the lowest. In Fig. 3, the maximum enhancement ranged from 14% to 23%. At $x/D = 10.58$ and $Re = 2500$, Nu_x/Nu_{fd} was equal to (1.77–2.18) at (0–10.5) kV, resulting in 23% enhancement. However, at the same x/D location and $Re = 13\,000$, Nu_x/Nu_{fd} was equal to (1.18–1.35) at (0–10.5) kV, resulting in 14% enhancement.

Fig. 4 shows the variation of average Nusselt number with voltage for the five different values of Reynolds number considered in this study. The ordinate is the average Nusselt number, Nu_{ave}, divided by its corresponding fully developed value, Nu_{fd}, at the same Reynolds number. The horizontal lines in the plot represent the case of zero applied voltage and show the enhancement due to the development of the thermal-hydraulic boundary layer.

Review of the average Nusselt number indicates that, at $Re = 2500$ and (0–10.50) kV, $Nu_{ave}/Nu_{fd} =$ (2.25–2.39), giving a 6% enhancement. On the other hand, at $Re = 13\,000$ and (0–10.50) kV, $Nu_{ave}/Nu_{fd} =$ (1.38–1.49), resulting in 8% enhancement. It is noteworthy that the 23–14% seen in Fig. 3 represents the level of enhancement experienced by the data point near the tube end, while 6–8% of Fig. 4 is from the average value for the entire length of the test section. The difference of 6% and 8%, namely 2%, is well within the experimental uncertainty and they should not be used to determine the trend of enhancement with Re. While the enhancement decreases with Re for the local values, it is more reasonable to assume that the enhancement of the average values are nearly insensitive to Re.

Despite the lower values of Nu_{ave}/Nu_{fd} at higher Reynolds numbers, the heat transfer coefficient shows an increasing trend with voltage for turbulent flows at $Re = 10\,000$ and 13 000. At the lowest Reynolds number of 2500 (the uppermost horizontal line in Fig. 4), the enhancement slightly decreased first and then increased. Ohadi et al. [10] and Nelson et al. [22] found a similar trend at lower Reynolds numbers. However, as they used only three voltages, enhancements dropped at their higher voltages. They attributed this behavior to the fact

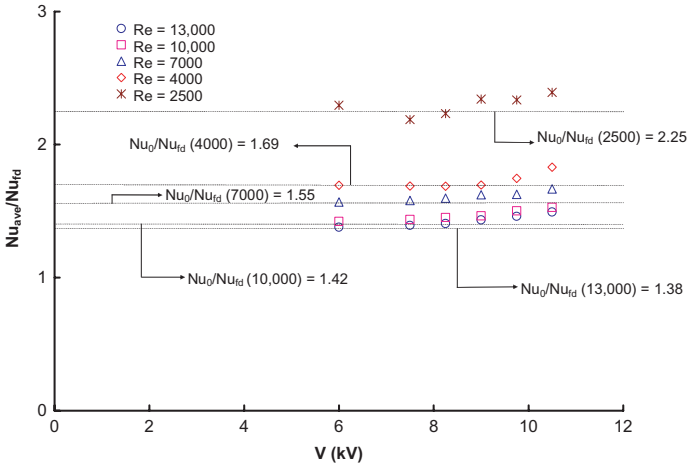

Fig. 4. Variation of the average Nusselt number with voltage; heat of electrode is not included.

that, as the voltage increases to a certain extent, ions spread uniformly in the entire domain, suppressing the corona wind effect. The heat transfer coefficient would be enhanced again when there was non-uniformity in the field. This effect was absent in our data at higher Reynolds numbers as the ions were washed away by the flow and the field never attained a uniform distribution.

In the present research, we have not included the heat generated by the electrode, Q_c, to the wall heat flux, Q/A, as corona heating does not take place at the wall. Some of the published works, however, have added the corona heating to the wall heat transfer as $Q + Q_c$.

$$Nu_{ave} = \frac{(Q + Q_c) - Q_L}{A(T_{wall,ave} - T_{bulk,ave})}\left(\frac{D}{k}\right) \tag{8}$$

In this equation, Q, Q_c, and Q_L, are, respectively, the heat of the test section heater, the heat generated by corona current in the electrode, and the heat losses through the setup. In order to make a meaningful comparison, the average Nusselt numbers were calculated from Eq. (8) and are presented in Fig. 5. As seen from the plot, the enhancement increases with voltage for all Reynolds numbers, showing the effect of non-uniformity of the field. At $Re = 2500$ and (0–10.50) kV, Nu_{ave}/Nu_{fd} ranged from 1.7 to 3.23, indicating 90% enhancement. At the higher Reynolds number of $Re = 13000$ and (0–10.50) kV, Nu_{ave}/Nu_{fd} ranged from 0.97 to 1.38, indicating 42% enhancement.

The enhancement caused by corona wind in low-Re flows is now much more pronounced. This indicates that, at higher values of Re, the corona wind is overshadowed by turbulence and is less effective.

The present experiments were repeated for each case to ensure the data are reproducible and the observed

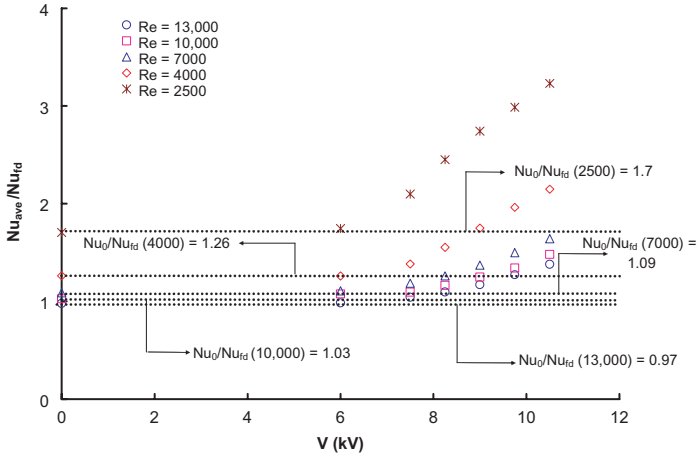

Fig. 5. Variation of the average Nusselt number with voltage; heat of electrode is included.

trends are not caused by the experimental uncertainty. Fig. 6 shows the data scatter at the lowest and highest values of Reynolds numbers used in this investigation. Uncertainty bars affixed to the data indicate that the data fall well within the uncertainty bands, and the estimates of experimental uncertainty are conservative.

The aforementioned heat transfer enhancements always occurred with some degree of pressure drop penalty. Fig. 7 shows the pressure drop along the test section tube at $Re = 2500$. The abscissa indicates the non-dimensional distance from the tube inlet. The ordinate is pressure coefficient defined by Eq. (6).

As expected, the increase in pressure drop is steep in the beginning owing to higher wall shear stress and fluid momentum change as the velocity develops to a fully developed profile. The pressure variations become nearly linear downstream. The data scatter and deviation from the overall trend seems to be due to experimental uncertainty, as the tube was smooth and the pressure drops were small. Based on our measurements,

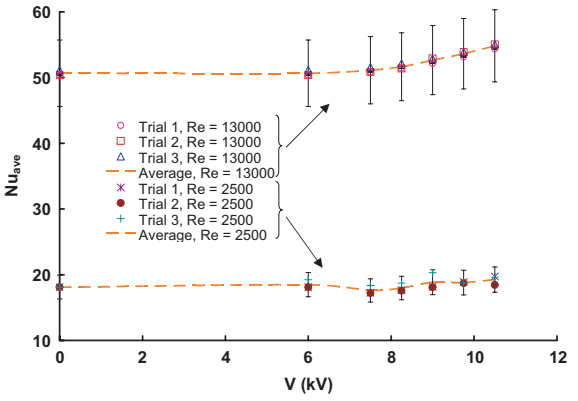

Fig. 6. Average Nusselt number vs. voltage.

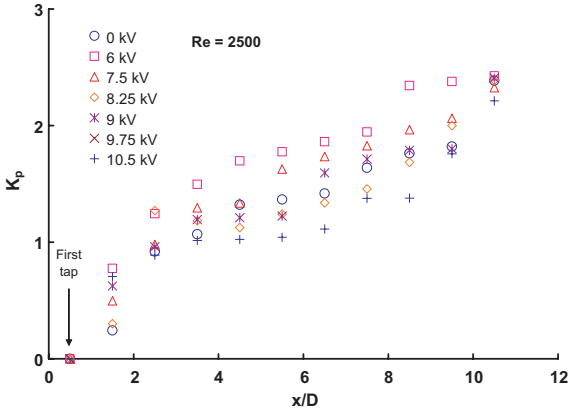

Fig. 7. Variation of local pressure drop at $Re = 2500$.

at high Reynolds numbers (not shown), the pressure data dropped close to the second pressure tap, and there was a pressure recovery close to the third tap. This could be due to a flow separation and re-attachment near the inlet. However, this trend was absent at low Reynolds numbers as the flow separation could have occurred much earlier.

Pressure drop increased up to a certain voltage, and then decreased in most cases, but the trend did not have a definite pattern. It was originally expected that the maximum pressure drop would occur at the highest applied voltage of 10.5 kV. But, this was not the case. It is assumed that the secondary motions are generated, but their effects are only felt in the radial direction. This can actually enhance the heat transfer coefficient and decrease the pressure drop, which is contrary to our expectations. It is noteworthy that corona discharge has been used to reduce the drag force for flow over flat plates [23]. In the present research, where the velocity boundary layer develops from the leading edge of the tube, the corona wind may be imparting momentum to air flow, thus reducing the pressure drop.

The results obtained in the present research are now compared with the existing literature. Three references are used for comparison. All three have studied heat transfer enhancement in pipe flows using corona discharge. Two of them dealt with the heat transfer enhancement in hydrodynamically fully developed region of tubes. This is different from the present research, where the measurements were made in the combined thermal-hydraulic developing region.

Ohadi et al. [10] studied heat transfer enhancement in tubes for hydrodynamically fully developed flow in transitional and turbulent regions. The range of Reynolds number of our work is very close to that used in [10], which allows a better comparison. However, the current–voltage (I–V) characteristic curves of the two studies are somewhat different. The range of voltages studied in the present case was much wider than that of [10]. Moreover, the maximum electric current of the electrode in the present work was 2.5 times that of [10]. The difference is caused by different pipe diameters used in the studies (25.4 mm in the present work and 31.75 mm in [10]), while the electrode diameters were both equal to 0.254 mm. The larger electrode-to-wall distance of [10] reduced the intensity of the electric field, resulting in lower currents and higher corona onset voltage.

The Nusselt numbers are compared in Fig. 8. As seen in the upper plot of the figure, the two sets of data have a good agreement in trends and magnitudes. The enhancement at lower Reynolds numbers is generally more sensitive to flow field, and the difference seen between $Re = 2500$ and 3000 data is possibly due to the difference in Re values. For all Reynolds numbers shown in the figure, the present data extend to higher voltages

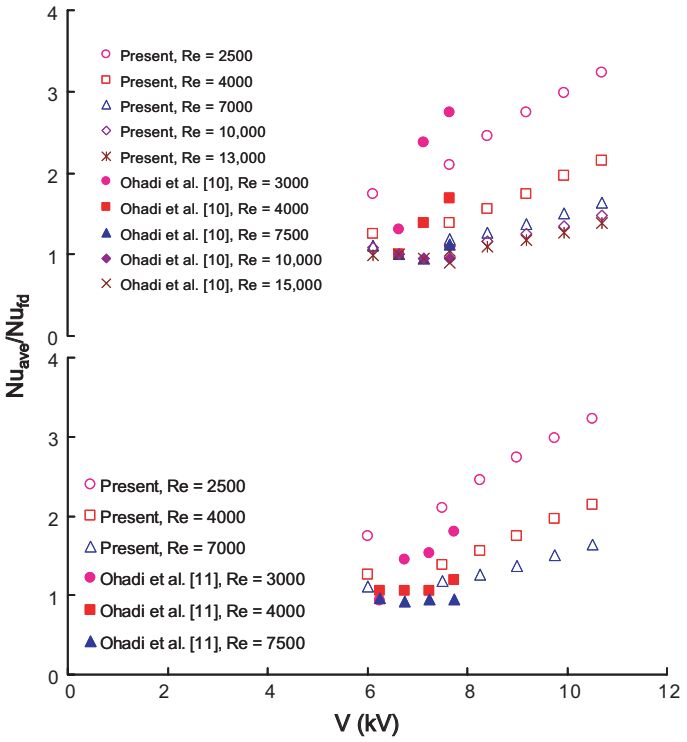

Fig. 8. Comparison of Nusselt number enhancement with the literature.

and provide higher heat transfer enhancement. This indicates that the electrode-to-wall distance plays an important role in the generation of corona wind and the level of enhancement.

Comparisons are also made with the data of [11] in Fig. 8, who studied the heat transfer enhancement in a shell-and-tube heat exchanger. The tube had a concentric electrode, just like the arrangement used in the present work. However, they had four electrodes placed radially apart on the shell side, which made their setup different. Regarding the I–V corona characteristics, the currents in the heat exchanger were much higher and the range of voltages was lower.

The Nusselt number enhancements for the present case are high even though the corona currents of [11] were higher. This could be because of the shell side excitation, which makes the arrangements different. However, the trends are similar.

The present research is also compared with the work of Nelson et al. [22]. Their work is an extension of [10]. Characteristic curves have not been presented in [22]. Hence, we only discuss the heat transfer enhancements.

For this comparison, we define the electric number as follows:

$$Ne = \left[\frac{I_0/(D\beta)}{\rho V^2}\right]^{1/2} \tag{9}$$

where Ne, I_0, D, β, ρ, and V are, respectively, electric number (ratio of electric body-force to inertia), electric current (A), tube diameter, ion mobility for positive ions (1.4×10^{-4} m^2/V s), fluid density (kg/m^3), and mean fluid velocity (m/s).

Comparison plots are given in Fig. 9. As seen in the figure, the heat transfer enhancement increases with the electric number. For a fixed Ne, the enhancement de-

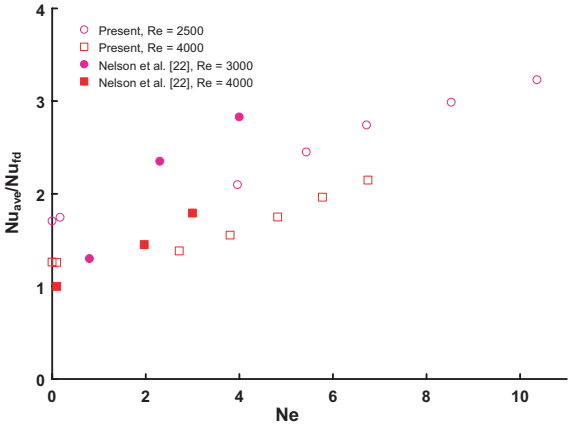

Fig. 9. Comparison of Nusselt number enhancement with the literature.

creases with *Re*, as the effect of electric body force diminishes. Both sets of data show similar trends, with the present results being lower at a given *Ne*. However, the present data extend to higher values of *Ne* and provide higher maximum enhancement for each Reynolds number. This may be attributed to the optimum electrode-to-wall distance of the present work that resulted in a wider range of the applied voltage.

6. Concluding remarks

This experimental research revealed the level of heat transfer enhancement that can be achieved by corona wind in the developing region of circular tubes. The electrode was a thin wire placed at the center of a tube and charged with DC high voltage. The study was performed in the transitional and the lower range of turbulent flows with $Re = 2500$–$13\,000$.

The maximum enhancement of the local heat transfer coefficient was obtained at the downstream end of the tube where the 0-kV heat transfer coefficient was the lowest. The level of enhancement decreased with Reynolds number. The maximum enhancement ranged from 14% at $Re = 13\,000$ to 23% at $Re = 2500$, both corresponding to the applied voltage of 10.5 kV.

The corona wind also increased the average heat transfer coefficient. The highest enhancement occurred at 10.5 kV, ranging from 6% to 8%, corresponding to $Re = 2500$ and $13\,000$, respectively. These values indicate the level of enhancement beyond the conventional (0-kV base) values in the developing region.

If the power of the electrode is added to the tube heat transfer, as is done by a number of investigators, the enhancement values will be much higher. In that case, enhancement of the average heat transfer coefficient at 10.5 kV ranged from 42% to 90%, corresponding to $Re = 13\,000$ and 2500, respectively. This shows that the level of enhancement strongly depends on whether the power of the electrode is included in the wall heat flux.

The results reported here are limited to the geometry and the range of parameters used in this investigation.

References

[1] A. Robledo-Martinez, Characteristics of DC corona discharge in humid, reduced-density air, J. Electrostat. 29 (1992) 101–111.

[2] P.A. Calva, F.P. Espino C., Threshold curves of the various modes of corona discharge in atmospheric air, IEEE Annual Report, Conference on Electrical Insulation and Dielectric Phenomena, Minneapolis, MN, 1997, pp. 612–615.

[3] L. Leger, E. Moreau, G. Touchard, Effect of a DC corona electrical discharge on the airflow along a flat plate, IEEE Trans. Industry Appl. 38 (6) (2002) 1478–1485.

[4] P.J. McKinney, J.H. Davidson, D.M. Leone, Current distributions for barbed plate-to-plate coronas, IEEE Trans. Industry Appl. 28 (6) (1992) 1424–1431.

[5] J.S. Chang, F. Pontiga, P. Atten, A. Castellanos, Corona discharge characteristics of narrow co-axial wire-pipe discharge tubes with gas flow, Conference Record—IAS Annual Meeting (IEEE Industry Applications Society) 3, Manufacturing Systems Development and Applications Department, 1993, pp. 1887–1893.

[6] Y. Hoshino, H. Hayashi, F. Koike, Effect of airflow and isopar [trademark] vapor on corona discharge, J. Imaging Sci. Technol. 47 (1) (2003) 13–17.

[7] L. Fouad, S. Elhazek, Effect of humidity on positive corona discharge in a three electrode system, J. Electrostat. 35 (1995) 21–30.

[8] A. Jaworek, A. Krupa, Corona discharge from a multipoint electrode in flowing air, J. Electrostat. 38 (1996) 187–197.

[9] A. Yehia, A. Mizuno, K. Takashima, Corona characteristics as influenced by magnitude and direction of the air flow rate in wire-duct reactor, in: Conference Record—IAS Annual Meeting (IEEE Industry Applications Society) 2, 2000, pp. 714–718.

[10] M.M. Ohadi, D.A. Nelson, S. Zia, Heat transfer enhancement of laminar and turbulent pipe flow via corona discharge, Int. J. Heat Mass Transfer 34 (4–5) (1991) 1175–1187.

[11] M.M. Ohadi, N. Sharaf, D.A. Nelson, Electrohydrodynamic enhancement of heat transfer in a shell-and-tube heat exchanger, Exp. Heat Transfer 4 (1) (1991) 19–39.

[12] Y. Tada, A. Takimoto, Y. Hayashi, Heat transfer enhancement in a convective field by applying ionic wind, J. Enhanced Heat Transfer 4 (2) (1997) 71–86.

[13] M.E. Franke, P.R.C. Hodge, Corona wind cooling of horizontal cylinders in air, in: Proceedings of the ASME–JSME Thermal Engineering Joint Conference 4, 1995, pp. 261–267.

[14] F.C. Lai, Effects of buoyancy on electrohydrodynamic-enhanced forced convection in a horizontal channel, J. Thermophys. Heat Transfer 12 (3) (1998) 431–436.

[15] H. Kalman, E. Sher, Enhancement of heat transfer by means of a corona wind created by a wire electrode and confined wings assembly, Appl. Thermal Eng. 21 (3) (2001) 265–282.

[16] S. Wangnipparnto, J. Tiansuwan, S. Jiracheewanun, T. Kiatsiriroat, C.C. Wang, Air side performance of thermosyphon heat exchanger in low Reynolds number region: with and without electric field, Energy Convers. Manage. 43 (14) (2002) 1791–1800.

[17] S. Kline, F. McClintock, Describing uncertainties in single-sample experiments, Mech. Eng. 75 (1953) 3–8.

[18] R.J. Moffat, Using uncertainty analysis in the planning of an experiment, ASME J. Fluids Eng. 107 (1985) 173–178.

[19] E.M. Sparrow, M. Molki, Turbulent heat transfer coefficients in an isothermal-walled tube for either a built-in or free inlet, Int. J. Heat Mass Transfer 27 (5) (1983) 669–675.

[20] W.M. Kays, M.E. Crawford, Convective Heat and Mass Transfer, third ed., McGraw-Hill, New York, 1993, p. 346.

[21] F.P. Incropera, D.P. DeWitt, Introduction to Heat Transfer, fourth ed., Wiley, New York, 2002, p. 460.

[22] D.A. Nelson, S. Zia, R.L. Whipple, M.M. Ohadi, Corona discharge effects on heat transfer and pressure drop in tube flows, Enhanced Heat Transfer 7 (1998) 81–95.
[23] S. El-Khabiry, G.M. Colver, Drag reduction by DC corona discharge along an electrically conductive flat plate for small Reynolds number flow, Phys. Fluids 9 (3) (1997) 587–599.
[24] K. Adiamiak, I.I. Inculet, G.S.P. Castle, The control of corona current distribution using shaped electrodes, J. Electrostat. 30 (1993) 381–392.
[25] S.H. Jeong, S.S. Kim, A study of electrohydrodynamic flow in a rectangular impactor with positive corona discharge, J. Am. Associat. Aerosol Res. 29 (1) (1998) 1–16.
[26] O.I. Kondratov, K.I. Kudyakov, I.P. Kuzhekin, A.E. Ostapenko, P.S. Shirikalin, Characteristics of impulse corona discharge current in an electrode system wire-cylinder, in: High Voltage Engineering Symposium, Conference Publication No. 467, 1999, pp. 3.244.P3–3.247.P3.
[27] K. Asano, R. Hishinuma, K. Yatsuzuka, Bipolar corona discharge from a floating filamentary particle between parallel plate electrodes, in: Conference Record—IAS Annual Meeting (IEEE Industry Applications Society) 1, 2000, pp. 606–609.
[28] M. Abdel-Salam, A. Hashem, A. Yeshiva, A. Mizuno, A. Turky, A. Gabr, Characteristics of corona and silent discharges as influenced by geometry of the discharge reactor, J. Phys. D 36 (3) (2000) 252–260.
[29] Y. Zebboudj, R. Ikene, Positive corona inception in HVDC configurations under variable air density and humidity conditions, Eur. Phys. J., Appl. Phys. 10 (3) (2000) 211–218.
[30] H. Toyota, S. Zama, S. Matsuoka, K. Hidaka, Gaseous characteristics in air and nitrogen at cryogenic temperature, IEEE Trans. Electrical Insulat. Dielectric Phenomena 9 (6) (2002) 891–898.
[31] A. Takimoto, Y. Tada, Y. Hayashi, K. Yamada, Convective heat transfer enhancement by a corona discharge, Heat Transfer: Jpn. Res. 20 (1) (1991) 18–35.
[32] M.D. Blanford, M.M. Ohadi, S.V. Dessiatoun, Compound air-side heat transfer enhancement in a cross-flow refrigerant-to-air heat exchanger, ASHRAE Trans. 101 (2) (1995) 1049–1054.
[33] H. Yang, F.C. Lai, Effects of Joule heating on EHD-enhanced natural convection in an enclosure, in: Conference Record of the IEEE Industry Applications, 3, 1997, pp. 1851–1858.
[34] M. Molki, M.M. Ohadi, B. Baumgarten, M. Hasegawa, A. Yabe, Heat transfer enhancement of airflow in a channel using corona discharge, Enhanced Heat Transfer 7 (2000) 411–425.
[35] C.C. Ngo, F.C. Lai, Effects of electric field on natural convection in an enclosure heated from below, in: Proceedings of the 35th National Heat Transfer Conference, Anaheim, CA, 2001, pp. 1–8.
[36] K.T. Tan, F.C. Lai, EHD-enhanced natural convection in an enclosure: effects of non-symmetric electric field, in: Proceedings of the 35th National Heat Transfer Conference, Anaheim, CA, 2001, pp. 1–9.
[37] N. Kasayapanand, J. Tiansuwan, W. Asvapoositkul, N. Vorayos, T. Kiatsiriroat, Effect of the electrode arrangements in a tube bank on the characteristics of electrohydrodynamic heat transfer enhancement: low Reynolds number, J. Enhanced Heat Transfer 9 (5–6) (2002) 229–242.